PHYSICAL REVIEW B **96**, 020406(R) (2017)

Information propagation in isolated quantum systems

David J. Luitz[1,2,*] and Yevgeny Bar Lev[3,†]

[1]*Department of Physics and Institute for Condensed Matter Theory, University of Illinois at Urbana-Champaign, Urbana, Illinois 61801, USA*

[2]*Department of Physics, T42, Technische Universität München, James-Franck-Straße 1, D-85748 Garching, Germany*

[3]*Department of Chemistry, Columbia University, 3000 Broadway, New York, New York 10027, USA*

(Received 20 March 2017; published 12 July 2017)

Entanglement growth and out-of-time-order correlators (OTOC) are used to assess the propagation of information in isolated quantum systems. In this work, using large scale exact time evolution we show that for weakly disordered nonintegrable systems information propagates behind a ballistically moving front, and the entanglement entropy growths linearly in time. For stronger disorder the motion of the information front is algebraic and subballistic and is characterized by an exponent, which depends on the strength of the disorder, similarly to the sublinear growth of the entanglement entropy. We show that the dynamical exponent associated with the information front coincides with the exponent of the growth of the entanglement entropy for both weak and strong disorder. We also demonstrate that the temporal dependence of the OTOC is characterized by a fast *nonexponential* growth, followed by a slow saturation after the passage of the information front. Finally, we discuss the implications of this behavioral change on the growth of the entanglement entropy.

DOI: 10.1103/PhysRevB.96.020406

Introduction. While the speed of light is the absolute upper limit of information propagation in both classical and quantum relativistic systems, surprisingly a velocity, which plays a similar role exists also for short-range interacting *nonrelativistic* quantum systems. This velocity, known as the Lieb-Robinson velocity, bounds the spreading of correlations in the system and implies that information about local initial excitations propagates within a causal "light cone," similarly to the light cone encountered in the theory of special relativity [1]. The shape of the light cone can be obtained from the correlation function

$$C_i^\beta(t) = -\frac{1}{Z}\mathrm{Tr}\, e^{-\beta\hat{H}}[\hat{A}_i(t), \hat{B}_{j=0}]^2, \tag{1}$$

where $\hat{H}$ is the Hamiltonian, β is the inverse temperature, $\hat{A}_i(t)$ and $\hat{B}_{j=0}$ are local Hermitian operators in the Heisenberg picture operating on sites i and $j = 0$, and $[.,.]$ is the commutator and $Z = \mathrm{Tr}\, e^{-\beta\hat{H}}$ is the partition function. For $\beta = 0$, Lieb and Robinson proved that for short-range interacting Hamiltonians this correlation function [which in that case is identical to the Frobenius norm of the commutator $[\hat{A}_i(t), \hat{B}_j]$ and is commonly known as the out-of-time-order correlator (OTOC)], is bounded by $C_i^\beta(t) \leqslant c\exp[-a(i - vt)]$, where a, c are constants and v is the Lieb-Robinson (LR) velocity. The OTOC was first introduced by Larkin and Ovchinnikov [2], who noted that it embodies a signature of classical chaos in the corresponding quantum system. In the semiclassical limit, the commutator is replaced by Poisson brackets and for the choice of the operators $\hat{A}(t) \to q(t)$ and $\hat{B} \to p$, gives $C^\beta(t) \sim \hbar^2(\partial q(t)/\partial q)^2$. The OTOC therefore measures the sensitivity of classical trajectories to their initial conditions, which for chaotic systems implies that the OTOC grows exponentially in time, $C^\beta(t) \sim \exp[2\lambda_L t]$, where λ_L is the classical Lyapunov exponent. A related manifestation of classical chaos in quantum systems was introduced in Ref. [3]. The time scale $t_d \sim \lambda_L^{-1}$ is a purely classical time scale, and quantum effects become appreciable only on a parametrically longer time scale known as the Ehrenfest time, $t_{\mathrm{Ehrenfest}} \sim \lambda_L^{-1}\ln[s_{cl}/\hbar]$, with the typical classical action s_{cl} [4–7]. For quantum systems without a proper semiclassical limit, the concept of Ehrenfest time does not directly apply, and the exponential growth of the OTOC, while plausible, cannot be similarly motivated. Moreover, for quantum systems with a finite local Hilbert space dimension it is easy to show that the OTOC is bounded from above uniformly in time. Indeed, the growth saturates after a time known as the "scrambling time," t_{sc} [8,9]. This creates an additional hurdle for the observation of the exponential growth of the OTOC in systems with a small local Hilbert space dimension, since the regime of exponential growth is pronounced only for times $t_d \ll t \ll t_{\mathrm{sc}}$. This difficulty can be remedied either by increasing the local Hilbert space dimension, or by studying OTOCs of extensive operators as recently proposed in Ref. [10].

The interest in OTOCs was revived by Kitaev [11,12], who using the AdS-CFT correspondence established a duality between some strongly coupled quantum systems and black holes [9,13–15]. The spreading of the OTOCs in space directly corresponds to the spreading of information on local excitations. Surprisingly, while transport in generic systems is diffusive, the LR bound suggests that information spreads behind a ballistically propagating front, namely that it resides within a linear light cone. This was observed in the study of the growth of the entanglement entropy, a global measure of quantum information, where it was conjectured that entanglement is transmitted "on contact," similarly to the spread of fire, and therefore inherently spreads faster than particles or energy [16]. The ballistic spreading of OTOCs was directly established and linked to combustion theory in Ref. [17]. In this work, a relation between the entanglement entropy growth and the spreading of the OTOC was also conjectured [17] (cf. Ref. [18] for a connection to the second Rényi entropy).

*david.luitz@tum.de

†yevgeny.barlev@columbia.edu

In this work, we examine the spreading of quantum information using both OTOCs and the entanglement entropy (EE) growth and establish the relationship between the two for diffusive and subdiffusive systems. We also provide a detailed analysis of the shape of the OTOCs in space and time.

Model. We study the one-dimensional spin-$\frac{1}{2}$ Heisenberg chain of length L in a random magnetic field,

$$\hat{H} = J \sum_{i=1}^{L-1} \vec{S}_i \cdot \vec{S}_{i+1} + \sum_{i=1}^{L} h_i \hat{S}_i^z, \tag{2}$$

with the coupling between the spins $J = 1$, and the random fields $h_i \in [-W, W]$ drawn from a uniform distribution with disorder strength W. This model exhibits an ergodic to nonergodic transition [19], which for infinite temperature occurs at $W_c \approx 3.7$ [20,21]. Interestingly, even in the nonergodic phase, where transport is completely frozen, information continues to spread logarithmically in time via dephasing [22], as was initially established using the growth of the EE [23,24] and later using OTOCs [18,25–31]. In contrast, the spreading of information in noninteracting Anderson insulators is completely frozen [32,33]. The ergodic phase of this model, occurring for $W < W_c$, exhibits anomalous subdiffusive spin transport characterized by a dynamical exponent varying continuously with disorder strength [34–44], but also a sublinear EE growth [36] (cf. Ref. [45] for a review). Here we focus solely on the ergodic phase and on the infinite temperature limit. In the weakly disordered limit, the disorder can be considered as an integrability breaking perturbation, allowing us to draw conclusions on generic *clean* systems. Here, information spread is bounded by normal linear light cones, as displayed in the left panel of Fig. 1. For stronger disorder, information is contained within *anomalously shaped* light cones, which are well described by power laws (see right panel of Fig. 1). Such anomalous light cones were previously predicted for the XY spin chain in a quasiperiodic potential [46], however to the best of our knowledge were never observed.

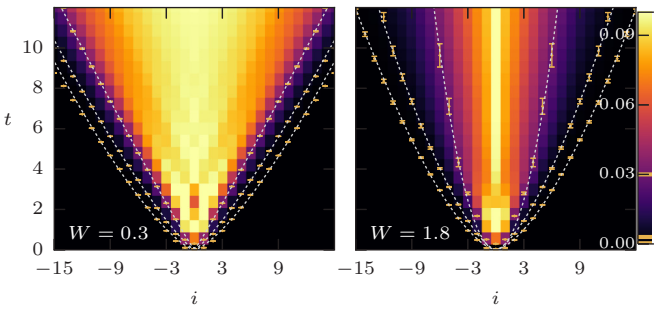

FIG. 1. OTOC [see Eq. (3)] for the $L = 31$ random Heisenberg chain in the $S_z = \frac{1}{2}$ sector at weak disorder $W = 0.3$ (left) and intermediate disorder $W = 1.8$ (right). At weak disorder, a linear light cone is visible (contour lines at three thresholds indicated on the color bar), which changes to a power-law light cone at intermediate disorder, with considerably slower information spreading. Here, we average over a modest number of disorder realizations ($n = 10$ for $W = 0.3$ and $n = 45$ for $W = 1.8$), but symmetrize the OTOC, effectively doubling the number of realizations.

Calculation of the OTOC. For the system (2), the OTOC can be simplified to

$$C_i^{\beta=0}(t) = \frac{1}{8} - \frac{2}{Z} \mathrm{Re\ Tr}\left(\hat{S}_i^z(t)\hat{S}_{j=0}^z \hat{S}_i^z(t)\hat{S}_{j=0}^z\right), \tag{3}$$

where to utilize the conservation of the total spin we take, $\hat{A}_i(t) = \hat{S}_i^z(t)$ and $\hat{B}_{j=0} = \hat{S}_{j=0}^z$. The numerical calculation of the correlation function in (3) for large enough system sizes is a challenging task and several approaches have been used previously, relying on the propagation of operators in the Heisenberg picture using either exact diagonalization (ED) of the Hamiltonian [27] or a representation in terms of matrix product operators (MPO) [47]. Although these approaches yield accurate results, they severely suffer from an exponential scaling with either system size (ED) or time (MPO). In order to alleviate these problems, we calculate the OTOC in the Schrödinger picture using an exact time-evolution with a Krylov space method [45,48,49]. Our method still scales exponentially in system size, however much larger system sizes can be reached compared to exact diagonalization of the Hamiltonian. In this work, we report results for system sizes up to $L = 31$ (cf. Fig. 1). To evaluate the trace in (3) we utilize Lévy's lemma and the concept of quantum typicality [45,50–52]. The trace is approximated by an expectation value with respect to a pure random state $|\tilde{\psi}\rangle$ drawn from the Haar measure, such that, $C_i(t) \approx \langle\tilde{\psi}|\hat{S}_i^z(t)\hat{S}_0^z\hat{S}_i^z(t)\hat{S}_0^z|\tilde{\psi}\rangle$. As was shown by Lévy, the error of this approximation is inversely proportional to the dimension of the Hilbert space if the operator can be written as a Lipshitz continuous function on a hypersphere on which the state is represented as a point. It is convenient to calculate independently $|\psi_1(t)\rangle = \hat{S}_i^z(t)\hat{S}_0^z|\tilde{\psi}\rangle$ and $|\psi_2(t)\rangle = \hat{S}_0^z\hat{S}_i^z(t)|\tilde{\psi}\rangle$, for various values of i. These calculations employ the exact propagation of a single wave function using a projection of the matrix exponential $\exp[-\mathrm{i}Ht]$ on the Krylov space of the Hamiltonian H (cf. Sec. V A of Ref. [45] for details). The OTOC is then given by the overlap $C_i(t) = \langle\psi_2(t)|\psi_1(t)\rangle$. While at each time step a full propagation back to time $t = 0$ is necessary, this procedure can be carried out efficiently, allowing us to access system sizes up to $L = 31$ (Hilbert space dimension 3×10^8).

Tomography of the OTOC. As explained in the introduction, the OTOC for two local operators with a fixed distance is expected to grow exponentially with time. In Fig. 2, we test this assertion for a number of distances and two disorder strengths. The growth of the OTOC shows two clear regimes: a fast initial growth, associated with the advance of the information front, followed by a slow saturation to the maximal value after the front has passed (bottom panels of Fig. 2). Surprisingly, the growth is not well described by an exponential, even for very weak disorder ($W = 0.3$), as is apparent from the logarithmic derivative on the upper panel of Fig. 2. This derivative monotonically decreases to zero, *without* a visible reversal trend for larger distances and longer times. For stronger disorder, within the subdiffusive phase, one might suspect either a stretched exponential [46] or a power law growth of the OTOC [18]. However, our data do not support these forms, possibly due to the very limited time range of their validity.

In Fig. 3, we study the spatial profile of the OTOC for fixed times. The LR bound establishes that the spatial decay

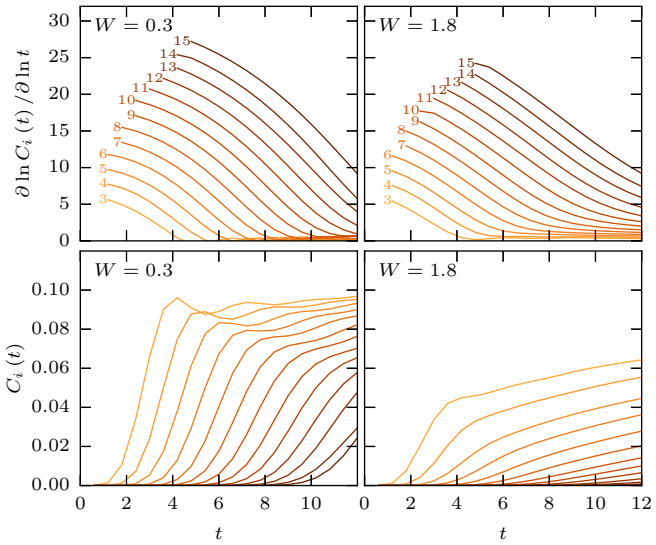

FIG. 2. OTOC at fixed distances (indicated by numbers) from the initial excitation in the middle of the lattice as function of time, for two disorder strengths $W = 0.3$ [$n = 10$] (bottom left) and 1.8 [$n = 45$] (bottom right). Darker colors represent longer distances, $x = 3{-}15$. Upper panels show the logarithmic derivative of the corresponding bottom panel. System size is $L = 31$.

of the OTOC should be *at least* exponential. In Fig. 3, we show the spatial profiles for different times (lower panels) and the corresponding semilogarithmic derivative in space (upper panels). The decay appears to be faster than exponential, suggesting that the LR bound is not saturated, however, for longer times and distances, the profile does appear to converge to an exponential form, which is more apparent for the case of stronger disorder.

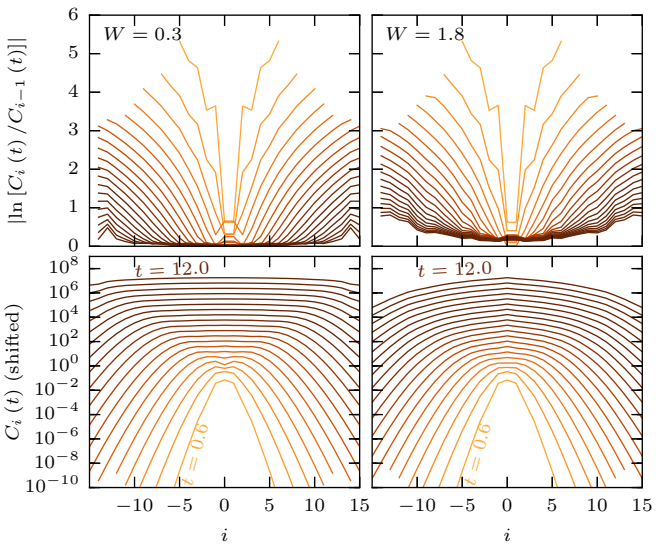

FIG. 3. OTOC at fixed times as function of site index, for two disorder strengths $W = 0.3$ [$n = 10$] (bottom left) and 1.8 [$n = 45$] (bottom right). Darker colors represent later times on a linear grid, $t = 0.6, \ldots, 12$, and the lines are shifted for clarity. Upper panels show the semi-logarithmic derivative of the corresponding bottom panel. System size is $L = 31$.

Light cone shape. A qualitative inspection of the OTOC in Fig. 1 reveals a presumably linear propagation of the OTOC front at weak disorder and a sublinear propagation at stronger disorder. To confirm this observation quantitatively, we extract the contour lines of the OTOC, $C_i(t) = \eta$, as a function of space and time for different thresholds, $10^{-4} < \eta < 10^{-1}$ [the OTOC in (3) is bounded from above by 0.125]. The contour lines are obtained from the times at which the OTOC exceeds the threshold η at each lattice site, and the statistical error is estimated by a bootstrap resampling. Motivated by the usual algebraic relation between space and time, which applies for diffusive and subdiffusive systems, we assume such a relation also for the shape of the contour lines, $x \sim t^{\alpha}$. Typical results for different thresholds are shown in Figs. 1 and 4 with very good fits to this form. Since the domain of the fits is clearly restricted in both space and time, we proceed by assessing the finite size effects. The left panels of Fig. 4 show that contour lines obtained for the same threshold η but different system sizes agree well within error bars. The right panels of Fig. 4 show the exponent α as a function of the threshold for various system sizes. Here we observe a strong systematic dependence of the exponent on the value of the threshold, such that $\alpha(\eta)$ exhibits a maximum at a threshold of the order of $\eta \approx 10^{-2}$. Finite size effects are the strongest for very large and very small thresholds, where the power-law fits are severely

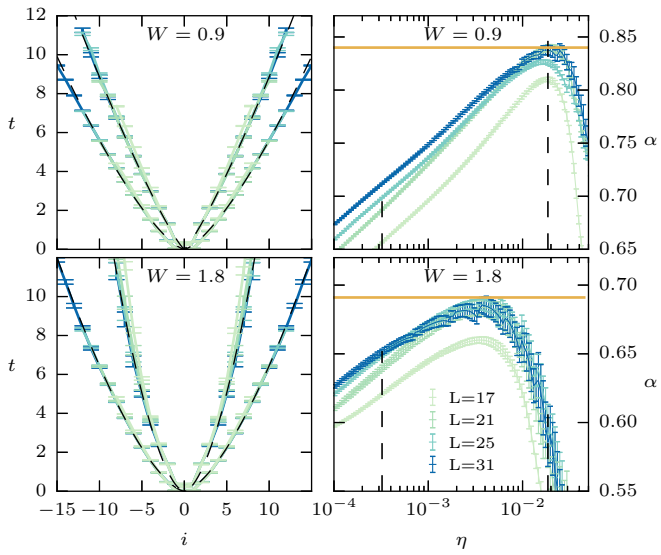

FIG. 4. (Left column) Extraction of the dynamical exponents from the shape of the OTOC "light cones" for two disorder strengths $W = 0.9$ and 1.8 [$n > 100$, except for $L = 31$, where we used the same realizations as shown in Fig. 1], two thresholds (3.24×10^{-4} and 0.0186, corresponding to the two distinctive groups of colored lines on each panel) and various system sizes, $L = 17$, 21, 25, and 31 (larger sizes correspond to more intense color). The dashed black lines are power law fits to the contour lines. The dependence of the extracted dynamical exponent on the threshold is plotted on the right column, for same disorder strengths and system sizes. The dashed black line here marks the thresholds used for the data on the left column, the orange solid line represents the final selection of the dynamical exponent, which does not depend on the size of the system asymptotically. Error bars represent the statistical errors in the extraction of the contours or the exponents, correspondingly.

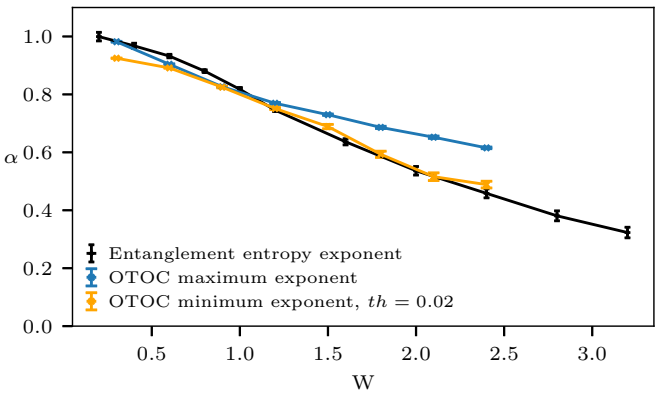

FIG. 5. Dynamical exponent relating space and time as extracted from the shape of the OTOC "light cones" for a system size of $L = 25$ (blue line), and the spread of the entanglement entropy (black line). The dynamical exponent for the entanglement entropy was taken from Ref. [36] for $L = 28$. Error bars indicate the statistical uncertainty and do not include systematic errors. As the exponent depends on the choice of the threshold, we show the maximal exponent as well as the exponent of the front propagation for large threshold ($\eta = 0.02$).

bounded either in space or in time. Hence we cannot exclude that $\alpha(\eta)$ is a monotonic function in the thermodynamic limit.

We interpret the maximal value of the dynamical exponent α as the *fastest mode of information spreading* in the system, corresponding to the propagation of the tail of the OTOC, and extract its value for different disorder strengths W [see Fig. 5 (blue)]. The error bars in this figure are statistical and do not include systematic errors, such as finite size effects. We observe a monotonously decreasing exponent as a function of disorder strength, starting from a value close to $\alpha = 1$ at very weak disorder, consistent with a linear light cone. We compare this exponent to the dynamical exponent obtained from the growth of the EE as a function of time starting from a random product state (data is taken from Ref. [36]). While the two exponents match very well at weak disorder, they seem to deviate from each other starting from $W \approx 1$, suggesting that the tail of the light cone spreads faster than EE. Extracting the exponent α from contour lines obtained at a larger threshold $\eta = 0.02$ (or larger) *does* produce a reasonable match, indicating that the *EE spreads as the front of the OTOC*.

Discussion. We studied information spreading in a generic quantum system using the OTOC. We showed that at fixed distance, the temporal growth of the OTOC does *not* appear to have a finite regime of exponential growth neither for weak nor stronger disorder, even for larger system sizes or longer distances. This suggests that an exponential regime in *local* quantum systems without a semiclassical limit is either absent or very short. The spatial profile of the OTOC seems to decay *faster* than exponentially, indicating that the LR bound could be further improved. However, we note a weak trend towards an exponential profile at larger times and stronger disorder.

We demonstrated that information mostly resides within spatio-temporal light cones. For weak disorder, with diffusive transport, we obtain light cones of linear shape. For stronger disorder, information transport is suppressed, leading to a deformation of the linear light cone into a power-law form, consistent with the previously observed subdiffusive transport as well as with the sublinear algebraic growth of the EE after a quench from a random product state. We directly compared the dynamical exponents extracted from the tail and the propagating front of the OTOC. While our data suggests that the tail of the OTOC propagates *faster* than the EE, the propagation of the front of the OTOC and the EE coincide. Unlike the EE, the front of the OTOC thus provides a glimpse into the local structure of information propagation in the system.

We also demonstrated that the growth of the OTOC is markedly different *before* and *after* its front passes through a given point in space. A fast initial growth is followed by a much slower saturation to the maximal value of the OTOC. This observation, combined with the association between the EE growth and the propagation of the OTOC front, which follows from our work, allows us to explain the apparent slowing down of the initial fast growth of the EE, starting from a product state, that was observed in a number of studies. We argue that this slow saturation regime of both the EE and OTOC occurs for times $L^{1/\alpha} < t < t_{\mathrm{Th}}(L)$ (where t_{Th} is the generalized Thouless time, which scales algebraically with system size [44]) and is a consequence of the conservation laws in the system. It is therefore expected to be absent for systems without any conservation laws, such as certain Floquet systems. We leave the study of information propagation in this regime for future work.

Acknowledgments. Y.B. would like to thank Igor Aleiner for many enlightening and helpful discussions. Y.B. acknowledges funding from the Simons Foundation (Grant No. 454951, D. R. Reichman). This work was supported by the Gordon and Betty Moore Foundation's EPiQS Initiative through Grant No. GBMF4305 at the University of Illinois. This research is part of the Blue Waters sustained-petascale computing project, which is supported by the National Science Foundation (Awards No. OCI-0725070 and No. ACI-1238993) and the state of Illinois. Blue Waters is a joint effort of the University of Illinois at Urbana-Champaign and its National Center for Supercomputing Applications. Our code uses the libraries PETSc [53–55] and SLEPc [49].

[1] E. H. Lieb and D. W. Robinson, Commun. Math. Phys. **28**, 251 (1972).

[2] A. I. Larkin and Y. N. Ovchinnikov, JETP **28**, 1200 (1969).

[3] R. A. Jalabert and H. M. Pastawski, Phys. Rev. Lett. **86**, 2490 (2001).

[4] G. Berman and G. Zaslavsky, Physica A **91**, 450 (1978).

[5] B. V. Chirikov, F. M. Izrailev, and D. L. Shepelyansky, Sov. Scient. Rev. C **2**, 209 (1981).

[6] B. Chirikov, F. Izrailev, and D. Shepelyansky, Physica D **33**, 77 (1988).

[7] I. L. Aleiner and A. I. Larkin, Phys. Rev. E **55**, R1243 (1997).

[8] Y. Sekino and L. Susskind, J. High Energy Phys. 10 (2008) 065.
[9] J. Maldacena, S. H. Shenker, and D. Stanford, J. High Energy Phys. 08 (2016) 106.
[10] I. Kukuljan, S. Grozdanov, and T. Prosen, arXiv:1701.09147.
[11] A. Y. Kitaev, A simple model of quantum holography, Part 1, http://online.kitp.ucsb.edu/online/entangled15/kitaev/ (2015).
[12] A. Y. Kitaev, A simple model of quantum holography, Part 2, http://online.kitp.ucsb.edu/online/entangled15/kitaev2/ (2015).
[13] A. Georges, O. Parcollet, and S. Sachdev, Phys. Rev. Lett. **85**, 840 (2000).
[14] A. Georges, O. Parcollet, and S. Sachdev, Phys. Rev. B **63**, 134406 (2001).
[15] J. Maldacena and D. Stanford, Phys. Rev. D **94**, 106002 (2016).
[16] H. Kim and D. A. Huse, Phys. Rev. Lett. **111**, 127205 (2013).
[17] I. L. Aleiner, L. Faoro, and L. B. Ioffe, Ann. Phys. **375**, 378 (2016).
[18] R. Fan, P. Zhang, H. Shen, and H. Zhai, Sci. Bull. **62**, 707 (2017).
[19] D. Basko, I. L. Aleiner, and B. L. Altshuler, Ann. Phys. **321**, 1126 (2006).
[20] T. C. Berkelbach and D. R. Reichman, Phys. Rev. B **81**, 224429 (2010).
[21] D. J. Luitz, N. Laflorencie, and F. Alet, Phys. Rev. B **91**, 081103 (2015).
[22] M. Serbyn, Z. Papić, and D. A. Abanin, Phys. Rev. Lett. **110**, 260601 (2013).
[23] M. Žnidarič, T. Prosen, and P. Prelovšek, Phys. Rev. B **77**, 064426 (2008).
[24] J. H. Bardarson, F. Pollmann, and J. E. Moore, Phys. Rev. Lett. **109**, 017202 (2012).
[25] R.-Q. He and Z.-Y. Lu, Phys. Rev. B **95**, 054201 (2017).
[26] Y. Chen, arXiv:1608.02765.
[27] X. Chen, T. Zhou, D. A. Huse, and E. Fradkin, Ann. Phys. (Berlin) **529**, 1600332 (2016).
[28] B. Swingle and D. Chowdhury, Phys. Rev. B **95**, 060201(R) (2017).
[29] K. Slagle, Z. Bi, Y.-Z. You, and C. Xu, Phys. Rev. B **95**, 165136 (2017).
[30] D.-L. Deng, X. Li, J. H. Pixley, Y.-L. Wu, and S. Das Sarma, Phys. Rev. B **95**, 024202 (2017).
[31] Y. Huang, Y.-L. Zhang, and X. Chen, Ann. Phys. **529**, 1600318 (2016).
[32] E. Hamza, R. Sims, and G. Stolz, Commun. Math. Phys. **315**, 215 (2012).
[33] M. Friesdorf, A. H. Werner, M. Goihl, J. Eisert, and W. Brown, New J. Phys. **17**, 113054 (2015).
[34] Y. Bar Lev, G. Cohen, and D. R. Reichman, Phys. Rev. Lett. **114**, 100601 (2015).
[35] K. Agarwal, S. Gopalakrishnan, M. Knap, M. Müller, and E. Demler, Phys. Rev. Lett. **114**, 160401 (2015).
[36] D. J. Luitz, N. Laflorencie, and F. Alet, Phys. Rev. B **93**, 060201 (2016).
[37] S. Gopalakrishnan, K. Agarwal, E. A. Demler, D. A. Huse, and M. Knap, Phys. Rev. B **93**, 134206 (2016).
[38] R. Vosk, D. A. Huse, and E. Altman, Phys. Rev. X **5**, 031032 (2015).
[39] A. C. Potter, R. Vasseur, and S. A. Parameswaran, Phys. Rev. X **5**, 031033 (2015).
[40] D. J. Luitz, Phys. Rev. B **93**, 134201 (2016).
[41] V. K. Varma, A. Lerose, F. Pietracaprina, J. Goold, and A. Scardicchio, J. Stat. Mech. (2017) 053101.
[42] M. Žnidarič, A. Scardicchio, and V. K. Varma, Phys. Rev. Lett. **117**, 040601 (2016).
[43] I. Khait, S. Gazit, N. Y. Yao, and A. Auerbach, Phys. Rev. B **93**, 224205 (2016).
[44] D. J. Luitz and Y. Bar Lev, Phys. Rev. Lett. **117**, 170404 (2016).
[45] D. J. Luitz and Y. Bar Lev, Ann. Phys. **529**, 1600350 (2017).
[46] D. Damanik, M. Lemm, M. Lukic, and W. Yessen, Phys. Rev. Lett. **113**, 127202 (2014).
[47] A. Bohrdt, C. B. Mendl, M. Endres, and M. Knap, New J. Phys. **19**, 063001 (2017).
[48] A. Nauts and R. E. Wyatt, Phys. Rev. Lett. **51**, 2238 (1983).
[49] V. Hernandez, J. E. Roman, and V. Vidal, ACM Trans. Math. Softw. **31**, 351 (2005).
[50] S. Popescu, A. J. Short, and A. Winter, Nat. Phys. **2**, 754 (2006).
[51] S. Goldstein, J. L. Lebowitz, R. Tumulka, and N. Zanghì, Phys. Rev. Lett. **96**, 050403 (2006).
[52] P. Reimann, Phys. Rev. Lett. **99**, 160404 (2007).
[53] S. Balay, W. D. Gropp, L. C. McInnes, and B. F. Smith, in *Modern Software Tools in Scientific Computing*, edited by E. Arge, A. M. Bruaset, and H. P. Langtangen (Birkhäuser Press, Boston, MA, 1997), pp. 163–202.
[54] S. Balay, S. Abhyankar, M. F. Adams, J. Brown, P. Brune, K. Buschelman, V. Eijkhout, W. D. Gropp, D. Kaushik, M. G. Knepley, L. C. McInnes, K. Rupp, B. F. Smith, and H. Zhang, *PETSc Users Manual*, Tech. Rep. ANL-95/11 - Revision 3.5 (Argonne National Laboratory, 2014).
[55] S. Balay, S. Abhyankar, M. F. Adams, J. Brown, P. Brune, K. Buschelman, V. Eijkhout, W. D. Gropp, D. Kaushik, M. G. Knepley, L. C. McInnes, K. Rupp, B. F. Smith, and H. Zhang, PETSc Web page, http://www.mcs.anl.gov/petsc (2014).